

# Preliminary results of a non-spherical aerosol method for the retrieval of the atmospheric aerosol optical properties

F.J. Olmo\*, A. Quirantes, A. Alcántara, H. Lyamani, L. Alados-Arboledas

*Dpto. Física Aplicada, Universidad de Granada, Fuentenueva s/n, 18071-Granada, Spain*

---

## Abstract

There is experimental evidence that the non-sphericity of certain atmospheric particles can cause scattering properties different from those predicted by standard Mie theory. Numerous studies indicate the need to consider the presence of non-spherical particles in modeling the optical properties of atmospheric aerosols. On the other hand, natural aerosols show a great variety of shapes, making difficult a realistic choice of a particle shape (or shape mixture) model. In this paper, we test a parameterization of the particle shape in the retrieval of size distribution, phase function, single scattering albedo and asymmetry parameter from direct and sky-radiance measurements. For this purpose we have substituted the Kernel based on the Mie theory included in the model SKYRAD.PACK by one derived for non-spherical particles. The method is applied under different atmospheric conditions, including Saharan dust outbreak, polluted and local mineral episodes. We compare the results with those obtained by the well known spheroids algorithm used in the AERONET network.

© 2005 Elsevier Ltd. All rights reserved.

**Keywords:** Aerosol properties; Non-spherical particles; Aerosol models

---

## 1. Introduction

Tropospheric aerosols modify regional and global climate by scattering and absorption of solar radiation at visible wavelengths. Many difficulties in assessing the climatic effects of atmospheric aerosols arise because of the great spatial and temporal variability of their concentrations and physical and chemical properties. Thus, continuous monitoring of aerosol in extended networks is required. On the other hand, a large mass fraction of the atmospheric aerosols consists of irregular particles (i.e. mineral particles) resulting from different sources, and the light-scattering properties of an ensemble of small irregular particles can differ significantly from those of an ensemble of spheres [1]. Altogether, scattering measurements are currently available for a limited number of samples of mineral particles and only for a few specific compositions, size distributions, and wavelengths.

Ground-based sun-photometry is a simple and reliable tool for monitoring column-integrated optical properties of atmospheric aerosols. However, few numerical codes exist that can predict the atmospheric integrated optical properties based on particle shape [2]. In general, the computations developed to estimate

---

\*Corresponding author. Tel.: +34 948 240023; fax: +34 958 243214.

E-mail address: [fjolmo@ugr.es](mailto:fjolmo@ugr.es) (F.J. Olmo).

the aerosol perturbation are based on aerosol integral properties in the visible wavelengths, and can be derived from aerosol compositions and size distributions using appropriate assumptions. Measurements of sky radiance in spectral bands where gaseous absorption is minimal can be used to retrieve information about particle size distribution and optical characteristics. This information, retrieved from ground-based measurements, is representative of their properties averaged over the whole atmospheric column. Retrievals of the scattering phase function, including scattering angles larger than 90°, are important, since this angular range of scattering determines the aerosol effect on climate and is used for remote sensing. On the other hand, particle shape affects aerosol scattering at large angles 100–140°. The backscattering of non-spherical particles is usually less dependent on the scattering angle than for spherical particles. The difference between non-spherical and spherical scattering is near maximum at an angle of 120°.

Although there is sufficient experimental evidence that the non-sphericity of dust particles can cause scattering properties different from those predicted by the Mie theory, dealing with non-sphericity is far from completely resolved, and most aerosol retrievals algorithms are based on the Mie theory, e.g. [3,4].

In this paper, we test a preliminary parameterization of particle shape in columnar size distribution, phase function, single scattering albedo and asymmetry parameter retrievals from direct irradiance and sky radiance data measured at Granada. The method retrieves the optical properties of non-spherical aerosols based on the model of a mixture of randomly oriented, polydisperse spheroids.

## 2. Experimental site and instrumentation

For this work we use solar extinction (direct irradiance) and diffuse sky radiance measured with a CIMEL CE-318 sun-photometer at Granada, Spain (37.18°N, 3.58°W and 680 m a.m.s.l.). Granada is a non-industrialized, medium-size city, located in south eastern Spain. The city is situated in a natural basin surrounded by mountains with the highest mountain range located at southeast of the basin, Sierra Nevada range, including several peaks above 3000 m. A coastal range, in the southern part of the basin, with elevations in the range 1000–2000 m, separates the city from the Mediterranean coast. The continental conditions prevailing in this site are responsible for larger seasonal temperature differences, providing cool winters and hot summers. The area presents a low relative humidity regime. Most rainfall occurs during spring and wintertime. The summer is normally very dry, with few rainfall events in July and August. On the other hand, the area is also at a short distance, about 200 km away, from the African continent. The local aerosol sources are mainly heavy traffic in the rather narrow streets of the city together with the re-suspension of the material available on the ground, especially during the warm season when the reduced rainfall and soil dryness can increase the contribution of local mineral dust. Due to its location in the Mediterranean basin, Granada is influenced by two major aerosol source regions: Europe and the Western Mediterranean Basin, as a major source of anthropogenic pollutants, and North Africa, as a principal source of natural dust [5].

The CIMEL CE-138 sun-photometer used is part of AERONET network, instrument #18, and has been in continuous operation since August 2002, although its inclusion in AERONET data base started by December 2004. These standard sun/sky radiometers are described in detail by Holben et al. [6]; however, a brief description will be given here. This instrument measures solar transmissions, aureole and sky radiances through a large range of scattering angles. The solar transmission measurements are performed with a 1.2° field of view every 15 min at 340, 380, 440, 500, 670, 870, 940 and 1020 nm (nominal wavelengths) to retrieve the aerosol optical depth. The sky radiance measurements are carried out at 440, 670, 870 and 1020 nm by means of almucantar and principal plane observations.

In order to compare our inversion procedure with an independent retrieval procedure we have used the aerosol properties computed in the frame of AERONET (<http://aeronet.gsfc.nasa.gov/>, Granada site). The input data used for our algorithm were the raw data, satellite transmitted to AERONET and uploaded by ftp to our local server on the same day. This allows us the possibility to compare the retrieval of both algorithms using the same set of data.

## 3. Methods

In the new method the aerosol optical depth was derived from the total optical depth, obtained from direct sun-photometer measurements data using the appropriate calibration constant and subtracting the Rayleigh

optical depth, as well as the O<sub>3</sub> and NO<sub>2</sub> contributions [7]. First, we remove measurements contaminated by cloud, using the cloud screening method of Smirnov et al. [8]. Also, each almucantar measurement sequence requires that sky conditions not change significantly during this time. Thus, sky radiance measurements could only be performed under clear sky conditions. To assure these sky conditions, the difference between almucantar radiances from both sides of the Sun (symmetry) was used as a check for the homogeneity of sky conditions during the measurement process, discarding asymmetrical situations (differences >10%) associated with inhomogeneous atmospheric conditions or the presence of clouds. Additionally, these almucantar sky radiance measurements are restricted to solar zenith angles >60° (morning and late afternoon) in order to be able to measure the scattering phase function for scattering angles up to 120°.

We compute Rayleigh, NO<sub>2</sub> and O<sub>3</sub> optical depth and optical air mass corresponding to the different constituents from the equations provided by Gueymard et al. [9] (SMARTS2 2.9 versions). The Ozone column contents were taken from TOMS values (<http://toms.gsfc.nasa.gov>). The NO<sub>2</sub> columns contents were obtained from the midlatitude model atmospheres in LOWTRAN7 code [10]. Assuming that the errors on the gaseous transmissions in Rayleigh, O<sub>3</sub> and NO<sub>2</sub> bands and on the relative air mass are negligible, the total uncertainty in aerosol optical depth is <±0.02 [11]. On the other hand, the total uncertainty in aerosol optical depth and sky radiance measurements from AERONET data are <±0.01 and <±5%, respectively [6].

The information retrieved from sky radiance at large scattering angles requires accurate correction for the effects of multiple scattering and for the contribution of light reflected from the Earth's surface and scattered downward in the atmosphere. Nakajima et al. [4] developed and applied an inversion scheme, which consists of a radiative transfer code as well as linear and nonlinear inversion components, and that also includes accurate radiative transfer modeling to account for multiple scattering (SKYRAD.PACK code). Detailed descriptions of the algorithm are found in these works [4,12]. Summarizing the retrieval method, the monochromatic diffuse sky radiance  $E(\Theta)$  (W m<sup>-2</sup> μm<sup>-1</sup>) is determined as the solution of the radiative transfer equation,

$$E(\Theta) = Fm_o \Delta\Omega [\omega\tau P(\Theta) + q(\Theta)], \quad (1)$$

where  $F$  is the monochromatic direct irradiance,  $m_o$  is the optical air mass,  $\Delta\Omega$  is the solid angle of the sky radiometer,  $\omega$  is the single scattering albedo of the whole air mass,  $\tau$  is the total optical thickness (sum for aerosol and molecules),  $P(\Theta)$  is the total phase function at a scattering angle  $\Theta$ , and  $q(\Theta)$  represents the contribution from multiple scattering. For the inversion retrieval the method uses the relative diffuse sky radiance (normalized by direct irradiance),  $R(\Theta)$ , that is less affected by deterioration of the interference filters of the sun-photometer, i.e.,

$$R(\Theta) = \frac{E(\Theta)}{Fm_o \Delta\Omega} = \omega\tau P(\Theta) + q(\Theta) = \beta(\Theta) + q(\Theta), \quad (2)$$

where  $\beta(\Theta)$  is the total differential scattering coefficient, that is the sum of the scattering coefficients for aerosol and for molecules. The aerosol optical thickness,  $\tau_a(\lambda)$ , is defined as

$$\tau_a(\lambda) = \frac{2\pi}{\lambda} \int_{r_{\min}}^{r_{\max}} K_{\text{ext}}(x, \tilde{m}) v(r) d \ln r, \quad (3)$$

where  $x$  is the size parameter,  $v(r)$  (= dV/d ln r (cm<sup>3</sup> cm<sup>-2</sup>)) is the columnar volume spectrum (aerosol size distribution),  $m$  is the complex refractive index,  $K(x, m)$  is the kernel function, and  $r_{\min}$  and  $r_{\max}$  are minimum and maximum aerosol radii. The kernel function  $K_{\text{ext}}$  is defined as

$$K_{\text{ext}}(x, \tilde{m}) = \frac{3}{4} \frac{Q_{\text{ext}}(x)}{x}, \quad (4)$$

where  $Q_{\text{ext}}$  is the extinction efficiency. Also, in this method, the aerosol differential scattering coefficient is expressed as

$$\beta_A(\Theta) = \frac{2\pi}{\lambda} \int_{r_{\min}}^{r_{\max}} K(\Theta, x, \tilde{m}) v(r) d \ln r, \quad (5)$$

where  $K$  is the kernel function.

The algorithm retrieves the columnar size volume distributions from  $\beta_A(\Theta)$  and  $\tau_a$  using an iterative inversion scheme. As the extinction coefficient can be expressed as the sum of scattering and absorption coefficients, aerosol optical thickness for the scattering can be obtained using Eq. (3) with the kernel function of scattering, and thus we can derive the monochromatic single scattering albedo [13].

Uncertainty analysis—sensitivity test—of the SKYRAD.PACK code can be seen in literature [4,12,13]. In our technique the inversion procedure uses the normalized sky radiance (almucantar and principal plane configuration) and the aerosol optical depth measured by means of a method that requires absolute calibration. The SKYRAD.PACK algorithm is based on spherical particle assumption. On the other hand, for the accurate retrieval of aerosol properties from sky radiance measurements, it is important to consider the influences of non-spherical particles [2,14]. In this paper, we modified this algorithm including a new parameterization for particle shape (spheroid particles) to calculate the extinction efficiency factor, the kernel function and the phase function. The method uses specified wavelengths, selected outside the gas absorption bands, in order to reduce the radiative transfer problem to a pure scattering problem. The connection between the optical measurements and the aerosol features occurs through the radiative transfer equation in a multiple-scattering scheme for a one-layer plane-parallel atmosphere [6]. All the available scattering angles in the range measured, which depend on the time of the day, were used to retrieve the aerosol volume distribution in the radius interval 0.06–10  $\mu\text{m}$ .

The EBCM, or  $T$ -matrix [15], theory has been used to calculate light scattering for non-spherical matrices (kernel matrices) instead of previously used Mie simulations by Nakajima [4,12,13]. Both incident and scattered electric fields can be expanded in vector spherical wave functions [16]. Incident and scattered expansion field coefficients can be related by means of a transition ( $T$ ) matrix, whose elements depend on the particle's size, shape and orientation. In the case of randomly oriented, axially symmetric particles, the  $T$ -matrix is calculated for the so-called natural reference frame ( $z$ -axis along the particle symmetry axis) and results are then averaged for all particle orientations [17]. Sizes of  $T$ -matrix have been chosen so that phase matrix elements are calculated with an accuracy of  $10^{-3}$ ; cross sections are accurate to within one part in  $10^4$  [18]. Accordingly, we defined in code the aerosol single-scattering properties as functions of the volume size distribution of randomly oriented polydisperse spheroids, and we computed the kernel matrices for randomly oriented prolate and oblate spheroids with aspect ratios ranging from 0.6 to 1.66, using equiprobable distributions, following the recommendations of Dubovik et al. [2]. In this preliminary work we have limited our estimations of the kernel matrices to particles where the size parameter is lower than 90.

For the complex refractive index the selected value is invariant with wavelength. The optimal value is retrieved by iteration and is that which minimize the residuals between measured and simulated normalized radiances. The equation of the residuals used is as follows:

$$\Delta = \sqrt{\frac{\sum_{\lambda,\Theta} [(R_{\lambda\Theta} - C_{\lambda\Theta})/R_{\lambda\Theta}]^2}{N_\lambda N_\Theta}}, \quad (6)$$

where  $R$  is the measured and  $C$  the calculated normalized experimental sky radiance, and  $N$  is the number of wavelengths and scattering angles measured.  $\lambda$  and  $\Theta$  refers the wavelength and the scattering angle, respectively. The refractive indices used in the iterative process are: 1.33–1.55 (0.02 step) and 0–0.01 (0.0005 step) for the real part and imaginary part, respectively. The algorithm retrieves first the real part of the refractive index—assuming the imaginary part as zero—and then, fixing the real part, the imaginary part is retrieved.

We assumed a Lambertian surface. Based on experience, to select the albedo value we have tested a range of values for the computations, and from the minimum residuals of the retrieved normalized irradiance data we found an optimal value [12]. The most favourable value that we have obtained is quite stable, and we can reasonably choose a constant value of 0.15 for Granada.

Finally, the procedure allows the retrieval of the complex refractive index, particle size distributions, single scattering albedo, phase function and asymmetry parameter. This method is applied to angular and spectral radiation measurements registered at Granada. The cases analysed correspond to different atmospheric conditions and air mass origins, including conditions influenced by desert dust, and we compare the results with the non-spherical method developed by Dubovik et al. [2] and used in AERONET network.

#### 4. Results

In order to verify how representative are the retrieval improvements of the new method we processed several measurements (extinction and sky radiance) collected at Granada in different atmospheric conditions during 2005 (January–July). In order to interpret correctly the aerosol optical properties retrieved, particularly the single scattering albedo and the asymmetry parameter, we have selected the cases with aerosol optical depth (670 nm) higher than 0.2. Kim et al. [13] suggest that, using the Nakajima code, the retrievals are more accurate if the aerosols are thick or solar zenith angle is large.

In this paper, we have selected three specific atmospheric situations produced during the first half of 2005 at Granada: Saharan episodes (16–18 March and 24 May–4 June), Europe–Atlantic-polluted episodes with predominance of small particles (31 January and 1–19 February) and episodes with predominance of local mineral particles due to the re-suspension of material available on the ground around the measurement site (5–20 April). Fig. 1 shows the representative backtrajectory analyses for 12 UTC of these atmospheric conditions. Back-trajectories were calculated with the HYSPLIT-4 model, available at the NOAA site <http://www.arl.noaa.gov/>, in order to interpret the different source regions of the air masses reaching the study area. To this end, 7 day isentropic back-trajectories at three different altitudes (500, 1500 and 3000 m a.g.l.) were obtained for each day. Fig. 1(a)—18 March 05—shows the arrival of a Saharan air mass at 500 and 3000 m a.g.l., conditions that are representative of those prevailing during 16–18 March and 24 May–4 June. Fig. 1(b)—19 February 05—shows the arrival of air masses coming from the Atlantic–Northern Europe (1500 and 3000 m a.g.l.) and from Europe (500 m a.g.l.), representing the conditions prevailing during the period from 31 January–19 February. The conditions prevailing during the predominance of local mineral particles—not shown—are characterized by regional re-circulation at 500, 1500 and 3000 m a.g.l.

Fig. 2 shows two examples of size distributions estimated for different times by both inversion codes (AERONET and the new method): Fig. 2(a) shows the comparison retrieved at 25 May 05, a case influenced by the Saharan air mass, and Fig. 2(b) shows the comparison retrieved at 1 February 05, a case influenced by the polluted air masses coming from Europe–Atlantic. Table 1 shows the statistical results retrieved for the different atmospheric situations by the two codes. The statistics shown have been calculated over all available individual distributions.

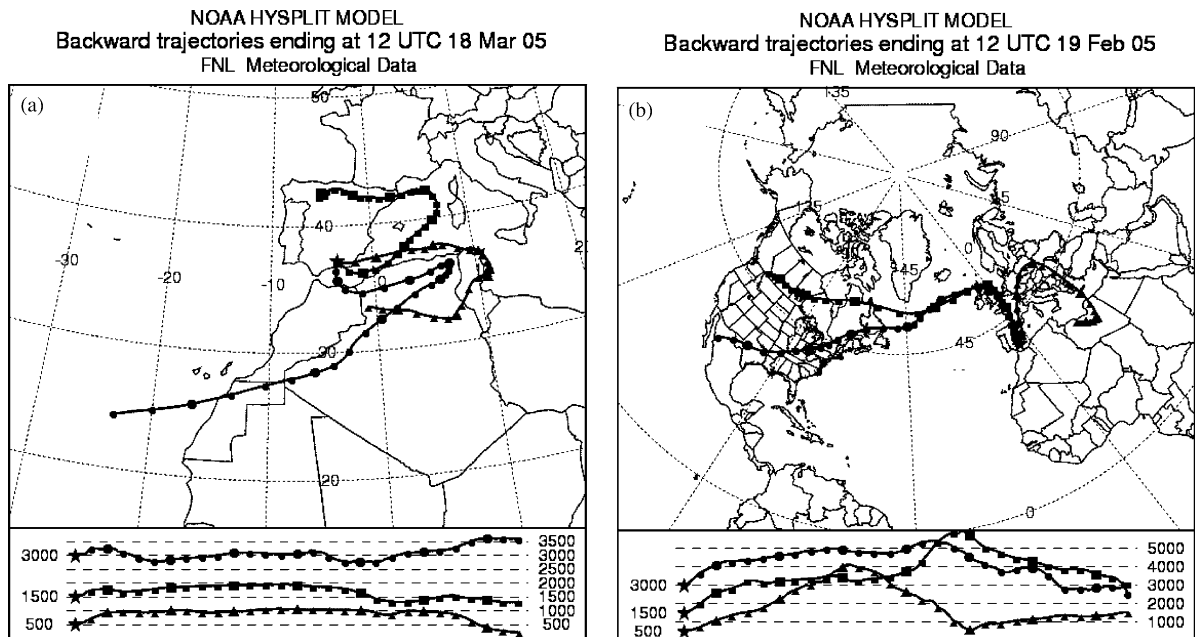


Fig. 1. Backtrajectories representatives of the atmospheric situation analysed: (a) Saharan dust event; (b) Polluted episode.

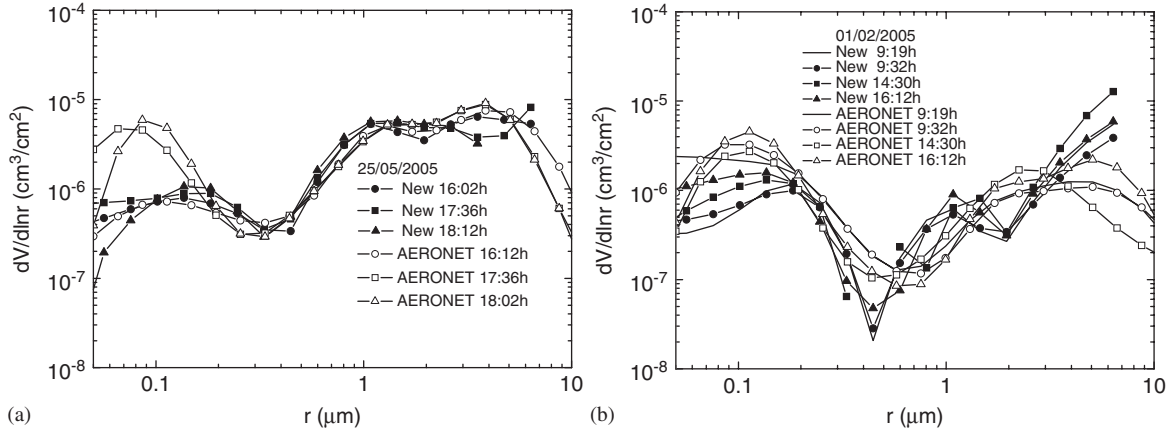


Fig. 2. Examples of size distributions retrieved at different times of two representative days: (a) Saharan dust event; (b) polluted episode.

Table 1

Mean values and root mean square deviation obtained using the two inversion methods

	AERONET	NEW	RMSD
<b>(a) Saharan dust episode</b>			
$V_{CT}$	$0.16 \pm 0.05$	$0.13 \pm 0.05$	0.05
$V_{C1}$	$0.05 \pm 0.02$	$0.020 \pm 0.007$	0.02
$V_{C2}$	$0.11 \pm 0.04$	$0.10 \pm 0.04$	0.03
$r_{eff1}$	$0.10 \pm 0.02$	$0.15 \pm 0.02$	0.05
$r_{eff2}$	$1.8 \pm 0.2$	$1.5 \pm 0.3$	0.33
<b>(b) Polluted episode</b>			
$V_{CT}$	$0.05 \pm 0.01$	$0.04 \pm 0.01$	0.01
$V_{C1}$	$0.03 \pm 0.01$	$0.020 \pm 0.003$	0.02
$V_{C2}$	$0.020 \pm 0.005$	$0.020 \pm 0.009$	0.01
$r_{eff1}$	$0.110 \pm 0.008$	$0.12 \pm 0.01$	0.01
$r_{eff2}$	$2.55 \pm 0.20$	$2.92 \pm 0.30$	0.49
<b>(c) Mineral local episode</b>			
$V_{CT}$	$0.08 \pm 0.03$	$0.08 \pm 0.03$	0.01
$V_{C1}$	$0.05 \pm 0.03$	$0.03 \pm 0.02$	0.02
$V_{C2}$	$0.040 \pm 0.007$	$0.04 \pm 0.01$	0.01
$r_{eff1}$	$0.14 \pm 0.03$	$0.18 \pm 0.01$	0.05
$r_{eff2}$	$2.0 \pm 0.3$	$2.1 \pm 0.6$	0.36

$V_{CT}$ —total volume concentration ( $\mu\text{m}^3 \mu\text{m}^{-2}$ ),  $V_{C1}$ —volume concentration of submicrometric mode ( $\mu\text{m}^3 \mu\text{m}^{-2}$ ),  $V_{C2}$ —volume concentration of micrometric mode ( $\mu\text{m}^3 \mu\text{m}^{-2}$ ),  $r_{eff1}$ —effective radius of submicrometric mode ( $\mu\text{m}$ ),  $r_{eff2}$ —effective radius of micrometric mode ( $\mu\text{m}$ ).

For the Saharan dust case, according to Fig. 2(a) and Table 1(a), we can observe that the two codes show similar results for the micrometric mode ( $>0.5 \mu\text{m}$ ) and marked differences for the submicrometric mode ( $<0.5 \mu\text{m}$ ). The retrieved submicrometric mode exhibits significant differences (artificially increased fine mode, according to [2,13]) in the individual distributions using the AERONET code, showing a very fluctuating pattern. By contrast, the results of the new code do not show such an artificially increased fine mode at 25 May 05, showing similar size distributions of the submicrometric mode along the day. These discrepancies may be due to the independent algorithm for the AERONET or invariant complex refractive index with wavelength in the algorithm used in this study [13]. On the other hand, we can appreciate good agreement in the micrometric range for both methods.

During the Saharan dust influence the size distributions obtained with the new method presents a mean effective radius around  $1.5 \pm 0.3 \mu\text{m}$  for the micrometric mode and an effective radius around  $0.15 \pm 0.02 \mu\text{m}$  for the submicrometric mode, while the AERONET method provides values of  $1.8 \pm 0.2$  and  $0.10 \pm 0.02$ , respectively, that means differences in the range 20% and 30%. The total volume concentration and the volume concentration of the micrometric mode retrieved show similar results for both codes (about 0.13 and 0.10 for the new method and about 0.16 and 0.11 for the AERONET method), but the volume concentration of the submicrometric mode is quite different (about 130% as average), mainly due to the artificially increased fine mode associated to the AERONET code. Dubovik et al. [2], using the AERONET code, also comment these retrieved artifacts in some experimental situations. Furthermore, the standard deviation of the volume concentration mean value of the submicrometric mode retrieved by the AERONET code is higher ( $\pm 0.02$ ) than that associated with the value retrieved by the new code ( $\pm 0.007$ ). Finally, the predominance of the dust particles associated with the enhancement of the micrometric mode is evident.

Fig. 2(b) shows a representative example of the size distributions retrieved using both codes on 1 February 05, where we assume that the contribution of the non-spherical particles is reduced. During the polluted episode the submicrometric mode presents an effective radius around  $0.110 \pm 0.008 \mu\text{m}$  for the AERONET code and  $0.12 \pm 0.01$  for the new code, showing a RMSD of about 12%. In this case the standard deviation associated with the AERONET code is lower. The micrometric mode effective radius shows values around  $2.55 \pm 0.20$  and  $2.92 \pm 0.30 \mu\text{m}$ , respectively. On the other hand, the volume concentrations show similar values for the AERONET and the new method, and the standard deviation being lower in the case of the new code for the submicrometric mode. This situation is rather different from those shown for the Saharan dust event. When the air mass came from Atlantic–Europe the influence of the submicrometric particles mode is evident. Under the Saharan dust influence (Fig. 2(a)) we obtain tri-modal size distributions with the two spheroids models, but in these last cases marked tri-modal distributions were obtained only with the new code. These last distributions (Fig. 2(b)) are in good agreement with measurements for a polluted atmospheric environment in urban area of northern hemispheric middle latitudes, where the total volume of micrometric mode particles presents a bimodal pattern, i.e. [13], and the fine mode particles are dominant volume contributors. While the volume concentration value of the micrometric mode is similar in both inversion methods, nevertheless the methods present different aspects in the size distributions (see Fig. 2(b)). The new code shows a mode around  $1 \mu\text{m}$  and the AERONET code shows this mode around  $2 \mu\text{m}$ . Finally, the RMSD shows values about 11% for the total volume concentrations and about 17% as maximum for the effective radius of the micrometric mode.

During the mineral local episode the results comparing both methods are also similar: presenting an effective radius for the submicrometric mode around  $0.14 \pm 0.03 \mu\text{m}$  (AERONET code) and  $0.18 \pm 0.01 \mu\text{m}$  (new parameterization). The micrometric mode shows values around  $2.0 \pm 0.3$  and  $2.1 \pm 0.6 \mu\text{m}$ , respectively. The total volume concentrations are the same ( $0.08 \pm 0.03$ ) and the standard deviation of the volume concentration associated with the AERONET code is lower in the case of the micrometric mode. The RMSD associated to the total volume concentrations and to the micrometric effective radius are about 12% as average.

One-way analysis of variance (ANOVA) can be employed to test whether or not the results of the two codes (populations) have the same mean [19]. One-way ANOVA assumes that the sample data sets have been drawn from populations that follow a normal distribution with constant variance. The null hypothesis is that the means of all selected data sets are equal. The alternative hypothesis is that the means of one or more selected data sets are different (not equal). We have used a significance level for comparison of 95%, and the ANOVA test is applied to the parameters shown in Table 1. In the case of the Saharan dust episodes, the population means of volume concentrations retrieved for the micrometric mode ( $V_{C2}$ ) are not significantly different. Moreover, in the case of the polluted episodes the population means of total volume concentrations ( $V_{CT}$ ) retrieved are not significantly different. For the rest of parameters, both for Saharan dust and polluted episodes, the test shows that the population means are significantly different. This fact is associated with the different shapes of the size distributions explained above. In the case of mineral local episode the ANOVA test shows that the population means of all the parameters are not significantly different.

Fig. 3 shows two examples of the aerosol phase function comparison retrieved for the codes in the case of desert dust influence (Fig. 3(a)) and polluted episode (Fig. 3(b)). As we can observe, the results agree well for sky-radiance aureole ( $<40^\circ$ ), the discrepancies between the two methods are small for scattering angles higher

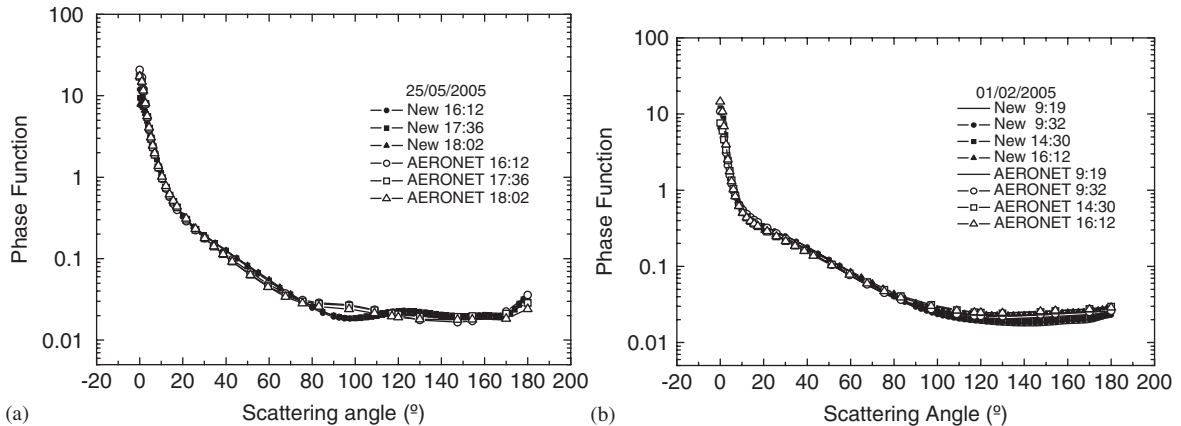


Fig. 3. Examples of phase functions (670 nm) retrieved at different times of two representative days: (a) Saharan dust event; (b) polluted episode.

Table 2

Mean values and root mean square deviation obtained using the two inversion methods

	440 nm	670 nm	870 nm	1020 nm	RMSD-Mean
<b>(a) Saharan dust episode</b>					
$\omega_{\text{AERONET}}$	$0.91 \pm 0.02$	$0.92 \pm 0.02$	$0.93 \pm 0.02$	$0.93 \pm 0.02$	0.02
$\omega_{\text{NEW}}$	$0.91 \pm 0.03$	$0.91 \pm 0.03$	$0.91 \pm 0.03$	$0.92 \pm 0.03$	
$g_{\text{AERONET}}$	$0.69 \pm 0.02$	$0.67 \pm 0.02$	$0.66 \pm 0.02$	$0.66 \pm 0.02$	0.02
$g_{\text{NEW}}$	$0.69 \pm 0.02$	$0.66 \pm 0.02$	$0.66 \pm 0.02$	$0.66 \pm 0.02$	
<b>(b) Polluted episode</b>					
$\omega_{\text{AERONET}}$	$0.93 \pm 0.03$	$0.90 \pm 0.04$	$0.88 \pm 0.05$	$0.87 \pm 0.05$	0.05
$\omega_{\text{NEW}}$	$0.94 \pm 0.02$	$0.90 \pm 0.03$	$0.86 \pm 0.03$	$0.85 \pm 0.04$	
$g_{\text{AERONET}}$	$0.63 \pm 0.01$	$0.53 \pm 0.02$	$0.51 \pm 0.03$	$0.50 \pm 0.03$	0.05
$g_{\text{NEW}}$	$0.62 \pm 0.03$	$0.56 \pm 0.03$	$0.55 \pm 0.02$	$0.56 \pm 0.02$	
<b>(c) Mineral local episode</b>					
$\omega_{\text{AERONET}}$	$0.95 \pm 0.01$	$0.95 \pm 0.02$	$0.94 \pm 0.02$	$0.94 \pm 0.02$	0.01
$\omega_{\text{NEW}}$	$0.95 \pm 0.02$	$0.95 \pm 0.03$	$0.93 \pm 0.04$	$0.93 \pm 0.04$	
$g_{\text{AERONET}}$	$0.71 \pm 0.06$	$0.65 \pm 0.03$	$0.62 \pm 0.01$	$0.60 \pm 0.01$	0.02
$g_{\text{NEW}}$	$0.72 \pm 0.03$	$0.66 \pm 0.03$	$0.63 \pm 0.01$	$0.63 \pm 0.01$	

$\omega$ —single scattering albedo,  $g$ —asymmetry parameter.

than 80° in the Saharan dust episode, and the results agree well for the different codes and scattering angles in the polluted event, taking into account that in these cases the non-spherical contribution is reduced. Discrepancies are due to the different particle shapes used in both methods. In addition, the retrieval artifacts in phase functions attributed to ignoring particle non-sphericity, when sky radiances were measured up to scattering angles of 80° [2], were significantly reduced in both codes.

Table 2 shows the mean values and the RMSD of the single scattering albedo and the asymmetry parameter retrieved by the two methods. As we can see the mean values of the two methods agree well during the different atmospheric conditions and wavelengths, also showing similar wavelength dependence. The standard deviation of the mean values is about 2–5% for the two models and the RMSD associated with all computed inversions (deviations between both methods) show values of about 2–3% for the Saharan dust episode, 5–7% for the polluted episode and 1–3% for the mineral local episode. The standard deviations and the RMSD of Table 2 show values lower than the accepted errors for these parameters in the inversion procedures, about 10–20% [6,13].

Finally, it is interesting to note the relatively good agreement of the two codes concerning the retrieval of single scattering albedo and asymmetry parameters in spite of the differences encountered in the retrieved size distributions (**Tables 1 and 2**). A possible explanation of this result is that the differences in the radiative transfer code used in each inversion procedure are responsible of differences in the “effective” size distributions obtained in each case, but after using one more time de radiative transfer codes to retrieve the single scattering albedo and asymmetry parameters the differences disappear by compensation effects.

## 5. Conclusions

We have developed a new inversion method, based in the SKYRAD.PACK code, to include the non-sphericity of aerosol particles as polydisperse, randomly oriented spheroids (equiprobable distributions of oblate and prolate), to retrieve the columnar aerosol optical properties from measurements of extinction and sky atmospheric radiances at Granada (Spain). Considering different atmospheric conditions (Saharan dust, pollution and local mineral events), the aerosol size distributions, the phase function, the single scattering albedo and the asymmetry parameter obtained have been compared with the results performed using the well known AERONET-spheroid model.

During the Saharan dust episodes the size distributions retrieved by the two codes show similar results for the micrometric mode ( $>0.5\text{ }\mu\text{m}$ ) and significant differences for the submicrometric mode ( $<0.5\text{ }\mu\text{m}$ ), with the AERONET code showing a widely fluctuating pattern due to an artificially increased fine mode. During the polluted episodes the size distributions retrieved by the two codes show differences for the micrometric mode (bimodal pattern with the new method). These discrepancies may be due to the independent algorithm for the AERONET or the invariant complex refractive index with wavelength in the algorithm used in this study. During the mineral local episodes the results comparing both methods are similar for the total volume concentrations, and micrometric volume concentrations and effective radius.

On the other hand, the phase functions obtained are similar, and the single scattering albedo and the asymmetry parameter show values with RMSD close to 1–7%. Finally, the spectral dependence of the single scattering albedo and the asymmetry parameter are also comparable in both methods.

This study is only a first attempt to explore the columnar aerosol optical properties with this new model. We also plan to explore different particle aspect ratios and compute more accurate spheroids kernel matrices which take into account size parameters close to 100–120 in order to account for the entire scattering signal. On the other hand, also following the recommendations described by Dubovik et al. [2], we will explore the particles aspect-ratio distributions that are fixed in our method.

## Acknowledgements

This work was supported by La Dirección General de Ciencia y Tecnología from the Education and Research Spanish Ministry through Projects REN 2003-03175 and CGL2004-05984-C07-03. We thank the AERONET staff for the data collection, calibration and processing. Also, we thank Professor T. Nakajima and colleagues for the software code SKYRAD.PACK and his help. Backward trajectories have been obtained by using the HYSPLIT-4, available at the NOAA site <http://www.arl.noaa.gov/>, and TOMS data, available by <http://toms.gsfc.nasa.gov/>.

## References

- [1] Volten H, Muñoz O, Rol E, de Haan JF, Vassen W, Hovenier JW, et al. Scattering matrices of mineral aerosol particles at 441.6 nm and 632.8 nm. *J Geophys Res* 2001;106(D15):17375–401.
- [2] Dubovik O, Holben BN, Lapyonok T, Sinyuk A, Mishchenko MI, Yang P, et al. Non-spherical aerosol retrieval method employing light scattering by spheroids. *Geophys Res Lett* 2002;29:N10.
- [3] Mishchenko MI, Hovenir JW, Travis LD. Light scattering by nonspherical particles. San-Diego: Academic Press; 2000. p. 690.
- [4] Nakajima T, Tonna G, Rao R, Boi P, Kaufman YJ, Holben BN. Use of sky brightness measurements from ground for remote sensing of particulate polydispersions. *Appl Opt* 1996;35(15):2672–86.
- [5] Rodríguez S, Querol X, Alastuey A, Kallos G, Kakaliagou O. Saharan dust contributions to PM10 and TSP levels in Southern and Eastern Spain. *Atmos Environ* 2001;35(14):2433–47.

- [6] Holben BN, Eck TF, Slutsker I, et al. AERONET—a federated instrument network and data archive for aerosol characterization. *Rem Sens Environ* 1998;66:1–16.
- [7] Alados-Arboledas L, Lyamani H, Olmo FJ. Aerosol size properties at Armilla, Granada (Spain). *Q J R Meteorol Soc* 2003;129:1395–413.
- [8] Smirnov A, Holben BN, Eck TF, Dubovik O, Slutsker I. Cloud-screening and quality control algorithms for the AERONET database. *Remote Sens Environ* 2000;73:337–49.
- [9] Gueymard C. Parameterized transmittance model for direct beam and circumsolar spectral irradiance. *Sol Energy* 2001;71:325–46.
- [10] Kneizys FX, Shettle EP, Abreu LW, Chetwind JH, Anderson GP, Gallery WO, et al. Users guide to LOWTRAN7, Environmental research paper 1010. Bedford, MA: US Air Force Geophys. Lab.; 1988.
- [11] Horvath H, Alados-Arboledas L, Olmo FJ, Jovanovic O, Gangl M, Kaller W, et al. Optical characteristics of the aerosol in Spain and Austria and its effect on radiative forcing. *J Geophys Res* 2002;107(D19):4386.
- [12] Boi P, Tonna G, Dalu G, Nakajima T, Olivieri B, Pompei A, et al. Calibration and data elaboration procedure for sky irradiance measurements. *Appl Opt* 1999;38(6):896–907.
- [13] Kim DH, Sohn B, Nakajima T, Takamura T, Takemura T, Choi B, et al. Aerosol optical properties over east Asia determined from ground-based sky radiation measurements. *J Geophys Res* 2004;109:D02209.
- [14] Dubovik O, Smirnov A, Holben BN, King MD, Kaufman YJ, Eck TF, et al. Accuracy assessment of aerosol optical properties retrieved from Aerosol Robotic Network (AERONET) Sun and sky radiance measurements. *J Geophys Res* 2000;105:9791–806.
- [15] Waterman PC. Symmetry, unitarity, and geometry in electromagnetic scattering. *Phys Rev* 1971;D3:825–39.
- [16] Tsang L, Kong JA, Shin RT. Theory of microwave remote sensing. New York: Wiley; 1985.
- [17] Mishchenko MI. Light scattering by randomly oriented axially symmetric particles. *J Opt Soc Am A* 1992;8:871–82 Errata, 1992; 9:497.
- [18] Mishchenko MI. Light scattering by size-shape distributions of randomly oriented axially symmetric particles of a size comparable to a wavelength. *Appl Opt* 1993;32:4652–66.
- [19] Neter J, Kutner M, Nachtsheim C, Wasserman W. Applied linear statistical models. Boston, MA: McGraw-Hill Inc.; 1996 Sections 16.8 and 16.9.